DOI 10.1007/s11182-020-01924-9

Russian Physics Journal, Vol. 62, No. 10, February, 2020 (Russian Original No. 10, October, 2019)

PHYSICS OF MAGNETIC PHENOMENA

MAGNETOCRYSTALLINE ANISOTROPY AND SPIN-ORIENTATION PHASE TRANSITIONS OF Co_2Z HEXAFERRITE DOPED WITH Ti^{4+} AND Zn^{2+} IONS

V. A. Zhuravlev, A. V. Zhuravlev, V. V. Atamasov, and G. I. Malenko UDC 538.62

The paper presents the methodology for calculation of ferromagnetic resonance spectra of polycrystalline and powder hexaferrites with easy magnetization plane. Magnitudes of magnetocrystalline anisotropy fields and magnetomechanical ratios of the hexaferrites of $Ba_3Co_{1.5+x}Ti_xFe_{24.5-2x}O_{41}$ *(0.0 ≤ x ≤ 1.0) and* $Ba_3Co_{2.5-x}Zn_xTi_{0.5}Fe_{23}O_{41}$ *(0.0 ≤ x ≤ 1.2) (0.0 ≤ x ≤ 1.2) systems were determined from an experimental study of the parameters of ferromagnetic resonance at room temperature. The study of temperature dependences of initial magnetic permeability was used to determine the temperatures of spin-orientation phase transitions of these materials. It was shown that substitution of* $Co^{2+}Ti^{4+}$ *complex for* Fe^{3+} *ions leads to the widening of the temperature region of existence for the magnetic ordering of the easy magnetization plane type with high magnetic permeability in the microwave frequency region. Substitution of* Zn^{2+} *ions for some of the* Co^{2+} *ions increases the saturation magnetization.*

Keywords: hexagonal ferrimagnetic material, ferromagnetic resonance, magnetocrystalline anisotropy, spin-orientation phase transitions, saturation magnetization.

INTRODUCTION

Oxide ferrimagnetics with a hexagonal crystalline structure (hexaferrites) are widely used in a variety of industries. According to the data presented in [1], one can currently see a considerable increase in the number of publications on physical properties and different aspects of hexaferrite application. Unique properties of hexaferrites are explained by high values of magnetocrystalline anisotropy (MCA) fields, saturation magnetization (M_S) and Curie temperature [2].

Hexaferrites with a positive first anisotropy constant have the magnetic order of the easy magnetization axis type (EMA). They are most frequently used to produce permanent magnets, magnetic recording media and radar-absorbing materials of the millimeter wavelength range. Hexaferrites with a negative first anisotropy constant have the magnetic order of the easy magnetization plane type (EMP). These materials have higher values of magnetic permeability in the microwave range than materials with EMA [2]. They are used to produce substrates for antennas, nonreciprocal microwave devices and broadband radar-absorbing materials and coatings.

In order to purposefully use hexaferrites, one needs to know the value and sign of MCA fields (H_a), as well as saturation magnetization (M_S). If there are monocrystalline hexaferrite samples, then measuring anisotropy fields by FMR method does not pose a problem [2–4]. However, ferrimagnetic materials are usually produced and used in the form of polycrystals or powders. Although such materials are macroscopically isotropic, there are three experimental

National Research Tomsk State University, Tomsk, Russia, e-mail: ptica@mail.tsu.ru; avzhur@gmail.com; atamasov.v@mail.ru; grisha-9708@mail.ru. Translated from Izvestiya Vysshikh Uchebnykh Zavedenii, Fizika, No. 10, pp. 162–169, October, 2019. Original article submitted June 21, 2019.

methods to determine the values of H_a: 1) law of approach to saturation (LAS) [5]; 2) singular point method [6, 7]; 3) ferromagnetic resonance method (FMR). The FMR method allows determining the values of magnetocrystalline anisotropy fields of materials both with EMA and EMP and the value of effective magnetomechanical ratio $\gamma = ge/2mc$. Here g is the effective g-factor of the examined material, e is the electron charge, m is the electron mass, c is the speed of light. It is preferable to use this method to determine H_a of materials that have higher values of anisotropy fields [8, 9].

A typical representative of hexaferrites with EMP is hexaferrite $Ba_3Co_2Fe_{24}O_{41}$ (Co_2Z) [2]. Replacing some of the bivalent cobalt ions with Fe^{2+} ions leads to noticeable decrease in the anisotropy field value in the base plane, which leads to the increase in magnetic permeability in the microwave range [2]. In addition to that, electron exchange between Fe^{2+} and Fe^{3+} ions increases the dielectric losses [2], which enhances the radar-absorbing properties of material. Due to that, our research sets the following tasks: suggest a technique for measuring the values of magnetomechanical ratios and anisotropy fields of hexaferrites with EMP; experimentally study the impact of substitution of $Co^{2+}Ti^{4+}$ complex for Fe^{3+} ions in hexaferrite $Ba_3Co_{1.5+x}Ti_xFe_{24.5-2x}O_{41}$ ($0.0 \le x \le 1.0$) and substitution of non-magnetic Zn^{2+} ions for some of the Co^{2+} ions in $Ba_3Co_{2.5-x}Zn_xTi_{0.5}Fe_{23}O_{41}$ hexaferrite ($0.0 \le x \le 1.2$) on temperatures of spin-orientation phase transitions and on magnetic anisotropy of these compounds.

DETERMINING THE MAGNETOCRYSTALLINE ANISOTROPY FIELDS OF MATERIALS WITH A HEXAGONAL CRYSTALLINE STRUCTURE FROM FMR EXPERIMENTS ON POLYCRYSTALLINE AND POWDER SAMPLES

Polycrystalline and powder materials are macroscopically isotropic, but the presence of MCA in individual grains is manifested on FMR curves as additional maximums and/or steps. For polycrystalline hexaferrites with high values of MCA fields, the approximation of non-interacting grains is implemented well. In this case the ratio $H_a > 4\pi M_S$ is fulfilled, and one can neglect the magnetic dipole interaction between the grains. Here H_a is the MCA field value, M_S is the saturation magnetization. The foundations of the FMR theory in approximation of non-interacting grains were developed by E. Schlömann for materials with cubic [10, 11] and hexagonal [12] crystalline structures. In publications [13, 14] this theory was generalized for the case of polycrystalline hexaferrites, taking into account the anisotropy of magnetomechanical ratio.

The starting point for this approach is calculating the FMR line of a monocrystalline single-domain grain shaped as an ellipsoid of revolution in the case of arbitrary orientation of the magnetization field ($\boldsymbol{H}_0$) in relation to the crystallographic axes of the grain. Then, averaging over all possible orientations of $\boldsymbol{H}_0$ is done to calculate the FMR curve of the polycrystal.

Let us assume that the sample consists of chaotically oriented identical particles shaped as an ellipsoid of revolution with hexagonal MCA. The density of the magnetic part of free energy (U) consists of contributions of Zeeman energy (U_{Zee}), energy of demagnetizing fields (U_M) and magnetocrystalline anisotropy energy (U_{MCA}). In the spherical system of coordinates, the density of free energy $U = U_{Zee} + U_M + U_{MCA}$ will be written as

$$U = -M_S H_0[\sin\Theta\sin\vartheta\cos(\Phi-\varphi) + \cos\Theta\cos\vartheta] + 2\pi M_S^2(N_\perp \sin^2\vartheta + N_\parallel \cos^2\vartheta)$$
$$+k_1\sin^2\vartheta + k_2\sin^4\vartheta + k_3\sin^6\vartheta + k_4\sin^6\vartheta\cos 6\varphi. \quad (1)$$

Here H_0 is the external magnetizing field, Θ, Φ are its polar and azimuthal angles, ϑ, φ are the polar and azimuthal angles of the magnetization vector, k_i are the MCA constants, $N_\perp, N_\parallel$ are the demagnetizing factors of the particle, $2N_\perp + N_\parallel = 1$. Anisotropy constant k_1 describes anisotropy in relation to the hexagonal axis $\boldsymbol{c}$, constants k_1, k_2, k_3 describe anisotropy in relation to the base plane, and constant k_4 describes anisotropy in the base plane of a monocrystalline grain.

At the first stage, equilibrium orientation angles of the magnetization vector (ϑ_0, φ_0) and resonance field values $H_0(\Theta, \Phi)$ are calculated by solving the system of three transcendental equations:

$$\begin{cases} \partial U / \partial \vartheta \big|_{\substack{\vartheta=\vartheta_0 \\ \varphi=\varphi_0}} = H_0[\sin\vartheta_0 \cos\Theta - \cos\vartheta_0 \sin\Theta \cos(\varphi_0 - \Phi)] \\ +0.5 \sin 2\vartheta_0 [H'_{a1} + H_{a2} \sin^2\vartheta_0 + (H_{a3} + (1/6) H_\Phi \cos 6\varphi_0) \sin^4\vartheta_0] = 0, \\ \partial U / \partial \varphi \big|_{\substack{\vartheta=\vartheta_0 \\ \varphi=\varphi_0}} = H_0 \sin\vartheta_0 \sin\Theta \sin(\varphi_0 - \Phi) - (1/6) H_\Phi \sin^6\vartheta_0 \sin 6\varphi_0 = 0, \\ [f / (\gamma / 2\pi)]^2 - H_1 H_2 + H_3^2 = 0. \end{cases} \tag{2}$$

The first two equations determine the equilibrium orientation of the magnetization vector and the third is the Smit–Suhl resonance equation. In equation (2) $H_{ai} = 2ik_i / M_S$ (i =1, 2, 3), $H_\Phi = 36k_4 / M_S$, $H'_{a1} = H_{a1} - 4\pi M_S \left(N_\parallel - N_\perp\right)$ are the anisotropy fields, f is the electromagnetic field frequency, $\gamma = ge/2mc$ is the magnetomechanical ratio. Values of H_1, H_2, H_3 are as follows:

$$\begin{gathered} H_1 = H_0[\sin\vartheta_0 \sin\Theta \cos(\varphi_0 - \Phi) + \cos\vartheta_0 \cos\Theta] + H'_{a1} \cos 2\vartheta_0 + \\ + H_{a2} \sin^2\vartheta_0 (4\cos^2\vartheta_0 - 1) + (H_{a3} + (1/6) H_\Phi \cos 6\varphi_0) \sin^4\vartheta_0 (6\cos^2\vartheta_0 - 1), \\ H_2 = H_0 (\sin\Theta / \sin\vartheta_0) \cos(\varphi_0 - \Phi) - H_\Phi \sin^4\vartheta_0 \cos 6\varphi_0, \\ H_3 = H_0 \cos\vartheta_0 (\sin\Theta / \sin\vartheta_0) \sin(\varphi_0 - \Phi) - H_\Phi \sin^4\vartheta_0 \cos\vartheta_0 \sin 6\varphi_0. \end{gathered} \tag{3}$$

The system of equations (2) is numerically solved by changing the magnetizing field angles in the ranges of $90° \geq \Theta \geq 1°$, $0° \leq \Phi \leq 30°$. These ranges of angle change are determined by the symmetry of MCA energy. As the practice of resonance curve calculation showed [13, 14], it is enough to change the angles with a step of $1°$. As a result of calculations, we get the matrix of equilibrium angle values $\vartheta_0(\Theta, \Phi)$, $\varphi_0(\Theta, \Phi)$ and resonance field values $H_0(\Theta, \Phi)$ for the given grid of magnetizing field angles. The resonance field for values $\Theta = 0°$, $0° \leq \Phi \leq 30°$ equals

$$H_0(0°, \Phi) = f / (\gamma / 2\pi) - H'_{a1}. \tag{4}$$

Imaginary part of the diagonal component of the magnetic permeability tensor of a monocrystalline grain is calculated based on formula [15]

$$\mu''(H, \Theta, \Phi) = \frac{\alpha(4\pi M_S) H_0(\Theta, \Phi)[H^2 + (1+\alpha^2) H_0^2(\Theta, \Phi)]}{[H^2 - (1+\alpha^2) H_0^2(\Theta, \Phi)]^2 + \left[2\alpha H H_0(\Theta, \Phi)\right]^2}. \tag{5}$$

Here H is the external magnetic field value, α is the damping constant in the Landau-Lifshitz-Gilbert equation of an individual grain. Imaginary part of magnetic permeability of a polycrystalline or powder sample is calculated by averaging (5) over the grid of angles Θ, Φ based on formula

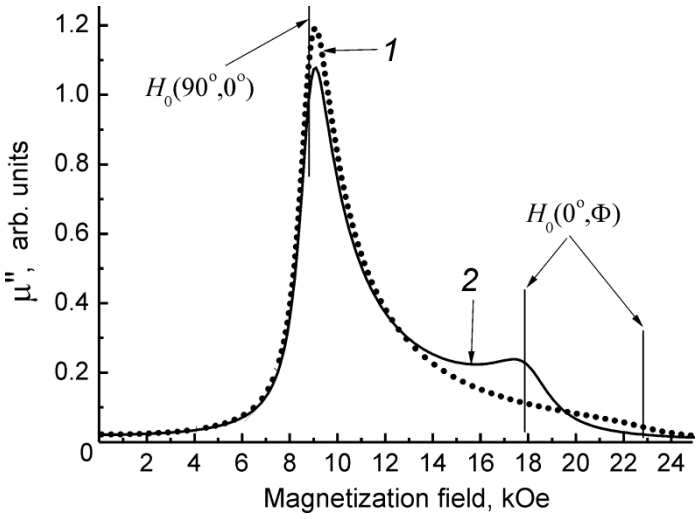

Fig. 1. Resonance curves of the polycrystalline hexaferrite with EMP: curve *1* (points) – anisotropy fields H_{a1} = –10 kOe, H_{a2} = H_{a3} = H_Φ = 0 kOe, curve *2* (solid) – anisotropy fields H_{a1} = –5 kOe, H_{a2} = –5 kOe, H_{a3} = H_Φ = 0 kOe.

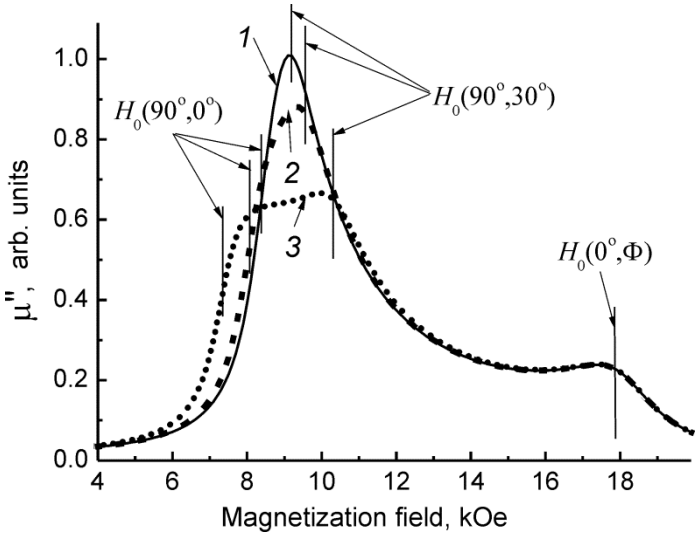

Fig. 2. Resonance curves of the polycrystalline hexaferrite with EMP: curve *1* – anisotropy fields H_{a1} = –5 kOe, H_{a2} = –5 kOe, H_{a3} = 0 kOe, H_Φ = 0.5 kOe, curve *2* – anisotropy fields H_{a1} = –5 kOe, H_{a2} = –5 kOe, H_{a3} = 0 kOe, H_Φ = 1 kOe, curve *3* – anisotropy fields H_{a1} = –5 kOe, H_{a2} = –5 kOe, H_{a3} = 0 kOe, H_Φ = 2 kOe.

$$\mu''_{poly}(H) = (3/2\pi)\int_0^{\pi/2}\int_0^{\pi/6}\mu''(H,\Theta,\Phi)\sin\Theta d\Theta d\Phi\,. \qquad (6)$$

The algorithm for calculating the imaginary part of magnetic permeability of a polycrystal based on formulas (2)–(6) was implemented in the form of the registered software program written in the Excel environment [16]. The results of calculating resonance curves by this method are presented in Fig. 1 and 2 for hexaferrites with EMP. FMR

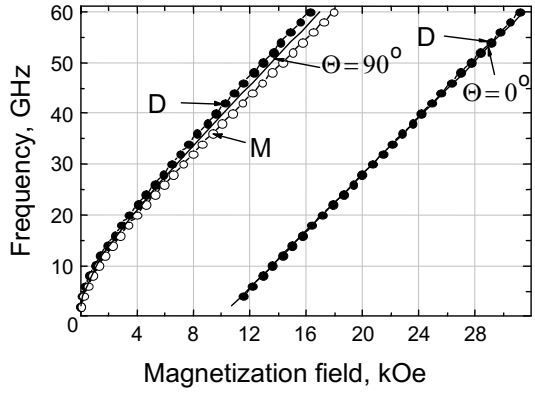

Fig. 3. FMR resonance frequencies for the material with EMP type anisotropy, $H_{a1} = -10$ kOe. Damping constant in the motion equation $\alpha = 0.1$, $\gamma = 2.8$ GHz/kOe.

curves in Fig. 1 were calculated without taking into account anisotropy in the base plane ($H_\Phi = 0$ kOe) and in Fig. 2 they were calculated for three values of H_Φ = 0.5, 1.0 and 2.0 kOe. Calculations were made for the following parameters: f = 36 GHz, M_S = 270 Gs, $\gamma/2\pi$ = 2.8 GHz/kOe, damping constant α = 0.07. Values M_S and α are characteristic for the materials, on which we experimented as described below. Vertical lines in Fig. 1 and 2 correspond to the resonance fields calculated based on formulas (4) and

$$[f/(\gamma/2\pi)]^2 = [H_0(90°,0°) + H_\Phi][H_0(90°,0°) - H_\Theta + H_\Phi/6],$$
$$[f/(\gamma/2\pi)]^2 = [H_0(90°,30°) - H_\Phi][H_0(90°,30°) - H_\Theta - H_\Phi/6]. \quad (7)$$

Here $H_\Theta = H'_{a1} + H_{a2} + H_{a3}$ is the anisotropy field in relation to the base plane.

According to Fig. 1, the presence of high-field singularity on the resonance curves near field $H_0(0°,\Phi)$ gives an opportunity to use formula (4) to determine the value of anisotropy field H'_{a1}. Estimation of anisotropy field H_Θ can be made using formulas (7) based on field $H_0(90°,0°)$ at $H_\Phi = 0$. Therefore, if in experiment one observes two singularities on the resonance curves in the fields close to $H_0(90°,0°)$ and $H_0(0°,\Phi)$, then one can identify the contribution from anisotropy fields of higher orders based on formula $H_{a2} + H_{a3} = H_\Theta - H'_{a1}$.

Fig. 2 shows the impact of anisotropy field H_Φ on the resonance curve shape. One can see that the value of this field can be estimated from experiment only for materials with $H_\Phi \geq 1$ kOe. For the examined materials the inverse inequality is true, that is why value H_Φ was not estimated from experiment.

Fig. 3 presents the results of comparison of the resonance curves of a polycrystal: maximums (M) on FMR curves and maximums of derivatives (D) with the calculation of the FMR resonance frequencies of a monocrystal (solid line) based on formulas (4) and (7) at $H_\Phi = 0$. One can see that in the case of polycrystals with EMP for the low-field singularity the best agreement with (7) is in the case of the average value of fields that correspond to the maximums of derivatives and maximums of FMR curves – $(H_D + H_M)/2$, for the high-field singularity it is with the maximum of derivative H_D.

Due to that, in order to determine the anisotropy fields, the experimental spectra of FMR of polycrystals are processed as follows [17]:

1. FMR curves are recorded within the set frequency range that depends on the value of anisotropy fields.

2. Then one plots the dependences of resonance frequencies on magnetization fields that correspond to the average value $(H_D + H_M)/2$ (low-field maximum) and maximum of derivatives (high-field maximum). These

dependences are processed by the least squares method based on formulas (7) and (4) to estimate the values of $\gamma/2\pi$ and approximate values of anisotropy fields H_{Θ}, H'_{a1}.

3. Then by means of thorough comparison of the shapes of the estimated and experimental FMR curves one can refine the values of magnetomechanical ratios and anisotropy fields.

EXPERIMENTAL SECTION

Production of samples and research methodology

Polycrystalline samples of hexaferrite $Ba_3Co_2Fe_{24}O_{41}$ (Co_2Z) and hexaferrites of the systems $Ba_3Co_{1.5+x}Ti_xFe_{24.5-2x}O_{41}$ ($0.0 \le x \le 1.0$), $Ba_3Co_{2.5-x}Zn_xTi_{0.5}Fe_{23}O_{41}$ ($0.0 \le x \le 1.2$) were synthesized according to the standard two-stage ceramic technology [1, 2]. Precursors were AR grade oxides and salts. Preliminary baking of samples compacted at 1000 atm was done in the air for 6 hours at the temperature of 1000ºC. Then they were ground in the ball mill, compacted again and baked for 10 hours at the temperature of 1280ºC.

The phase composition and crystalline lattice parameters of the powders were examined by X-ray diffraction method (SHIMADZU XRD-6000 polycrystalline diffractometer in Bragg-Brentano geometry equipped with a focusing pyrographite crystal monochromator). The PDF4+ computer database of X-ray powder diffractometry data of the International Centre for Diffraction Data (ICDD, Denver, United States) was used for the qualitative analysis of phase composition. Quantitative analysis of the phase composition was carried out using Powder Cell 2.4 computer software.

Resonator technique was used to study the FMR spectra in the frequency range of 25–38.5 GHz. Measurements were done on the automated spectrometer using the R2-65 panoramic VSWR meter. A rectangular multimode resonator of the 7.2×3.4 mm standard was used. It was 170 mm long and connected into the waveguide line in passing through mode. With this resonator length, 11 oscillation modes were observed in the above-indicated frequency range, with the antinode of the variable magnetic field in the resonator center. Measurements were done on the spherical samples with diameters from 0.8 to 1.0 mm at room temperature. The samples were placed in the center of the resonator. The error of anisotropy field value estimation was ±0.2 kOe, and for the magnetomechanical ratio ($\gamma/2\pi$) the error was ±0.02 GHz/kOe.

Temperature dependences of the initial magnetic permeability ($\mu_0(T)$) were measured using a measurement solenoidal transformer with two identical back-to-back secondary coils placed inside a primary coil. Measurements were carried out at the frequency of 10 kHz. Amplitude of the variable magnetic field inside the primary coil of the transformer was 1 Oe. The residual unbalance signal of the secondary coils was compensated before the measurements. Then a sample of the examined material, shaped as a parallelepiped with approximate dimensions 2×2×5 mm, was placed inside one of the secondary coils, and the whole structure was heated in the muffle furnace to a temperature exceeding Curie temperature. Dependences $\mu_0(T)$ were measured during temperature decrease after the transformer was taken out of the muffle furnace. The unbalance signal, proportionate to $\mu_0(T)$, was amplified and detected by the UNIPAN 223 selective nanovoltmeter. The sample temperature was measured using the differential copper-constantan thermocouple, one of the junctions of which was at 0°C, and the other – in contact with the examined sample. The detected signal and EMF of the thermocouple were digitized by ADC and processed on PC.

Examination of the magnetization curves and determination of the saturation magnetization value were done in the pulse magnetic fields on the unit described in [18].

Data of X-ray research on the synthesized materials

Synthesis temperatures for hexaferrites of different structural types: M, Y, W, Z etc. are close [1]. That is why it is rather difficult to synthesize the single-phase samples of one structural type, and materials usually contain additional hexagonal impurity phases.

The results of X-ray phase analysis of Co_2Z hexaferrite and some compositions of hexaferrites of the system $Ba_3Co_{1.5+x}Ti_xFe_{24.5-2x}O_{41}$ ($0.0 \le x \le 1.0$) are presented in Table 1, where all samples along with the target Z phase

TABLE 1. Results of X-Ray Phase Analysis of Hexaferrites

Phase content and lattice constant	Co_2Z	$Ba_3Co_{1.5+x}Ti_xFe_{24.5-2x}O_{41}$, concentration, x				
		0.0	0.3	0.4	0.6	0.8
Z phase,%	96.0	97.9	96.9	98.8	96.5	97.5
Y, W phases,%	4.0	2.1	3.1	1.2	3.5	2.5
c, Å	52.30	52.21	52.24	52.26	52.28	52.29

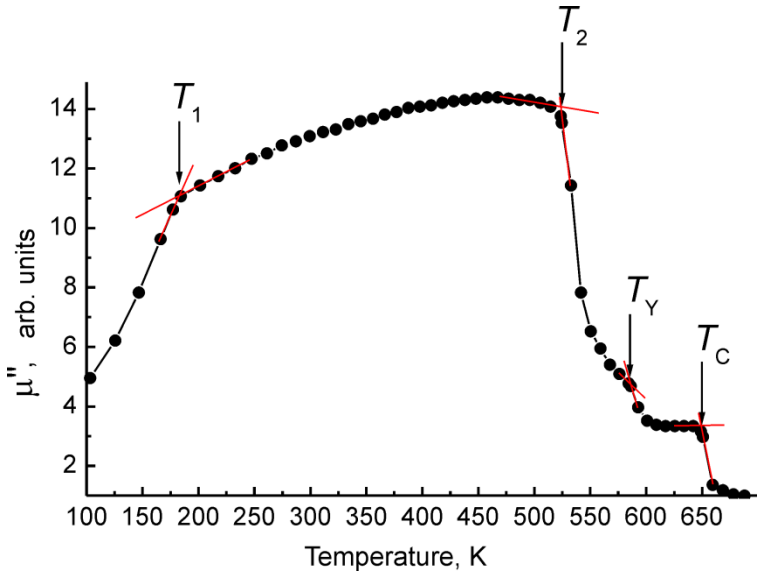

Fig. 4. Temperature dependence of initial magnetic permeability of Co_2Z hexaferrite: T_1 – temperature of EMC ↔ EMP transition, T_2 – temperature of EMP ↔ EMA transition, T_Y – Curie temperature of Y phase, T_C – Curie temperature of Z phase.

contain a small number of impurity Y and W phases. The lattice constant along the hexagonal axis (***c***) of Co_2Z hexaferrite corresponds to the data published in [1, 2]. The sample with x = 0.0, which is initial for the system $Ba_3Co_{1.5+x}Ti_xFe_{24.5-2x}O_{41}$, has a somewhat smaller lattice constant value c. Further on, when substituting the $Co^{2+}Ti^{4+}$ complex for some of the Fe^{3+} ions, c increases to the values corresponding to Co_2Z hexaferrite.

Hexaferrites of the system $Ba_3Co_{2.5-x}Zn_xTi_{0.5}Fe_{23}O_{41}$ have the phase composition that is similar to the data in Table 1. The content of the main Z phase is ≥ 95%, and the content of Y and W impurity phases is ≤ 5%. Lattice constant c does not depend on the substitution of x and equals ≈52.27 Å. This is due to the proximity of ionic radii of Co^{2+} and Zn^{2+} cations [19].

Spin-orientation phase transitions and MCA field of hexaferrite Co_2Z

Temperature dependence of the initial magnetic permeability $\mu_0(T)$ of hexaferrite Co_2Z is presented in Fig. 4. When the temperature increases from the liquid nitrogen temperature to the Curie temperature, several spin-orientation phase transitions (SOPT) occur [2]. The state of easy magnetization cone (EMC) is implemented in the temperature range of up to $T_1 \approx 182$ K. At temperature T_1 the spin-orientation phase transition from cone to EMP occurs. Then at $T_2 \approx 524$ K the transition from easy plane to EMA is observed. This transition occurs through the state with EMC that is implemented in the region with a sharp drop in $\mu_0(T)$. The state with EMA continues up until the Curie temperature $T_C \approx 650$ K. The estimation of transition temperatures was done by linear interpolation of dependence segments $\mu_0(T)$ near the inflection points. In Fig. 4 an arrow marked as T_Y indicates a step on the dependence $\mu_0(T)$ that corresponds to

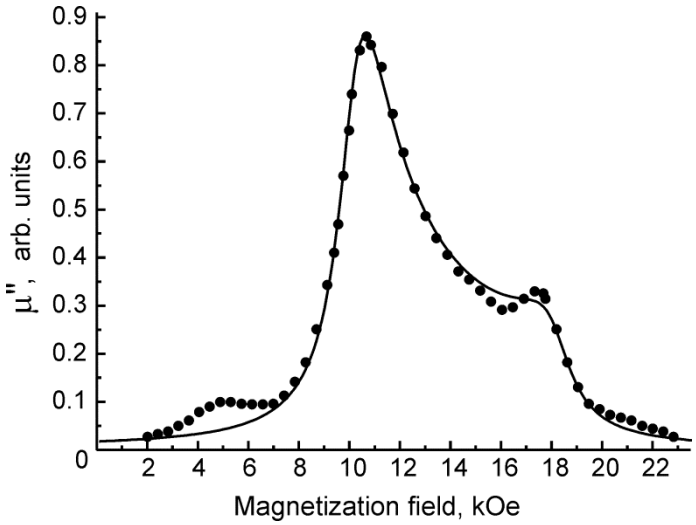

Fig. 5. Resonance curve of Co_2Z hexaferrite at the frequency of 38.32 GHz: the points stand for the experimental data, the solid line indicates the estimation for the following parameters of the material $\gamma/2\pi = 2.84$ GHz/kOe, $H'_{a1} = -4.7$ kOe, $H_{a2} = -3$ kOe, $H_{a3} = H_\Phi = 0$ kOe, $M_S = 270$ Gs, $\alpha = 0.07$.

the Curie temperature (≈585 K) of Y impurity phase. The obtained values of transition temperatures correlate with the data presented in [2]: $T_1 \approx 210$ K, $T_2 \approx 480$ K, $T_Y \approx 613$ K (for Co_2Y hexaferrite) and $T_C \approx 683$ K.

FMR curve of this hexaferrite measured at the frequency of 38.32 GHz is presented in Fig. 5. The points stand for the experimental data, the solid line is a theoretical curve estimated for the following material parameters: $\gamma/2\pi = 2.84$ GHz/kOe, $H'_{a1} = -4.7$ kOe, $H_{a2} = -3$ kOe, $H_{a3} = H_\Phi = 0$ kOe, $M_S = 270$ Gs, $\alpha = 0.07$. Let us mention that the value of anisotropy field $H_\Theta = H'_{a1} + H_{a2} + H_{a3} = -7.7$ kOe is noticeably smaller than the value provided in [2], i.e. $H_\Theta = -13$ kOe. However, research literature contains a remarkable variation of data on anisotropy field values H_Θ of Co_2Z hexaferrite (–9 ÷ –13 kOe) [20]. A small maximum on the resonance curve in the field $H \approx 5$ kOe can be due either to the effect of the domain structure on FMR or to the presence of traces of high-anisotropy Y or M phases.

Temperatures of spin-orientation phase transitions and MCA fields of hexaferrites of the system $Ba_3Co_{1.5+x}Ti_xFe_{24.5-2x}O_{41}$

Substitution of the $Co^{2+}Ti^{4+}$ complex for some of the Fe^{3+} iron ions in Co_2Z hexaferrite leads to the widening of the temperature range of EMP existence, which is important for development of thermally stable devices. The results of research on the magnetic phase diagram of hexaferrites of the system $Ba_3Co_{1.5+x}Ti_xFe_{24.5-2x}O_{41}$ ($0.0 \le x \le 1.0$) are presented in Fig. 6. The diagram is plotted based on the measurements of temperature dependences of the initial magnetic permeability. One can see that with the rise in x, there is an increase in the temperature of EMP ↔ EMA transition, while the Curie temperature goes down. These temperatures become equal at concentration $x \approx 0.7$. Temperature of EMC ↔ EMP transition goes down, i.e. the region of EMP existence expands. Magnetomechanical ratios and anisotropy fields of this hexaferrite system measured by FMR method are presented in Table 2.

According to Table 2, the values of magnetomechanical rations within the limits of the experiment error (±0.02 GHz/kOe) do not change, when x changes. With an increase in concentration of ions of the $Co^{2+}Ti^{4+}$ complex an increase in the values of anisotropy fields H'_{a1}, H_Θ occurs. One can identify the contribution from anisotropy fields H_{a2} into field H_Θ only for the values $x < 0.6$. Hexaferrite with $x = 0.5$ is not included in this table, because this composition is the initial one for the second examined system of hexaferrites.

TABLE 2. Magnetomechanical Ratios and MCA Fields of the System $Ba_3Co_{1.5+x}Ti_xFe_{24.5-2x}O_{41}$ ($0.0 \le x \le 1.0$)

Concentration, x	0.0	0.2	0.3	0.4	0.6	0.7	0.8	0.9	1.0
$\gamma/2\pi$, GHz/kOe	2.81	2.83	2.84	2.83	2.84	2.83	2.84	2.84	2.84
H_Θ, kOe	–10.3	–11.0	–11.8	–11.8	–12.1	–12.5	–12.5	–13.0	–14.0
H'_{a1}, kOe	–6.5	–8,7	–9,5	–9,8	–	–	–	–	–
H_{a2}, kOe	–2.5	–2.3	–2.3	–2.0	–	–	–	–	–

TABLE 3. Magnetomechanical Ratios and Anisotropy Fields of the System $Ba_3Co_{2.5-x}Zn_xTi_{0.5}Fe_{23}O_{41}$ ($0.0 \le x \le 1.2$)

Concentration, x	0.0	0.1	0.2	0.3	0.4	0.5	0.6	0.7	0.8	1.0	1.2
$\gamma/2\pi$, GHz/kOe	2.83	2.83	2.83	2.83	2.82	2.82	2.83	2.83	2.82	2.83	2.83
H_Θ, kOe	–11.5	–11.0	–11.1	–11.0	–10.0	–9.5	–10.5	–9.5	–9.5	–7.5	–6.7
M_S, Gs	247	253	257	262	266	270	274	277	281	288	293

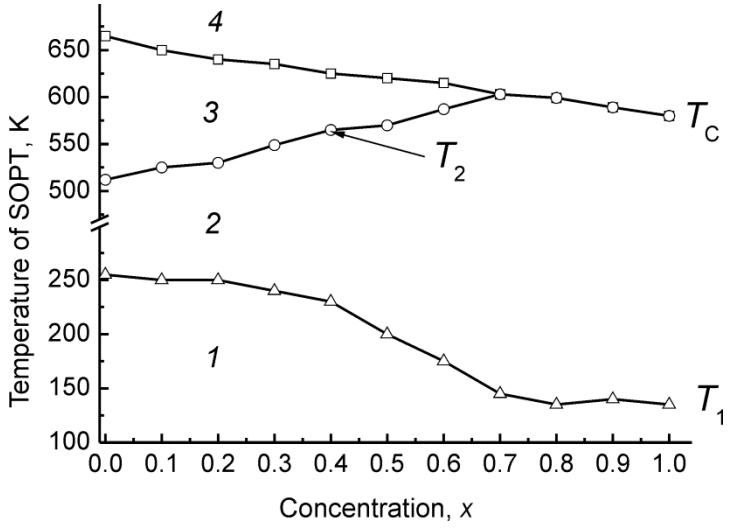

Fig. 6. Magnetic phase diagram of hexaferrites of the system $Ba_3Co_{1.5+x}Ti_xFe_{24.5-2x}O_{41}$ ($0.0 \le x \le 1.0$): *1* – region of EMC existence, *2* – region of EMP existence, *3* – region of EMA existence, *4* – paramagnetic state.

Spin-orientation phase transitions and magnetic characteristics of hexaferrites of the system $Ba_3Co_{2.5-x}Zn_xTi_{0.5}Fe_{23}O_{41}$

Magnetic phase diagram of hexaferrites of the system $Ba_3Co_{2.5-x}Zn_xTi_{0.5}Fe_{23}O_{41}$ ($0.0 \le x \le 1.2$) is presented in Fig. 7. One can see that the increase in the concentration of non-magnetic Zn^{2+} ions leads to the decrease in transition temperatures T_1, T_2, T_C. Linear decrease in the Curie temperature with the rise in non-magnetic substitution in hexaferrites $Ba_3(Co_{1-x}Zn_x)_2Fe_{24}0_{41}$ is noted in publications [2, 21]. According to Table 3, magnetomechanical ratios within the limits of measurement error do not depend on substitution of zinc ions for cobalt ions.

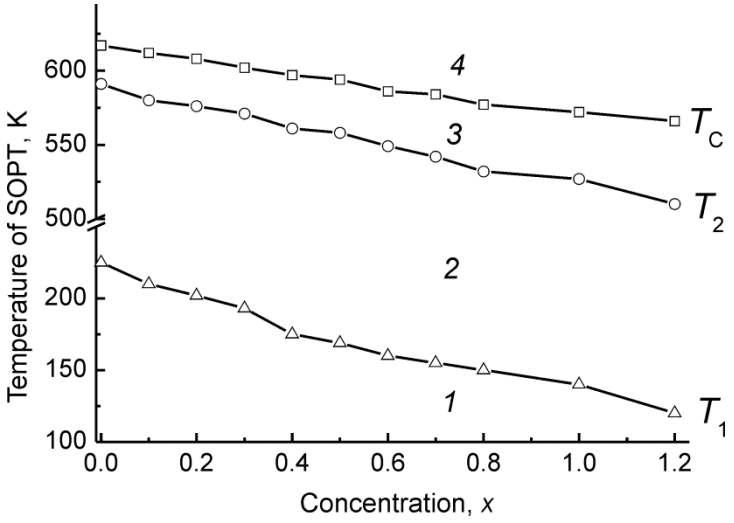

Fig. 7. Magnetic phase diagram of hexaferrites of the system $Ba_3Co_{2.5-x}Zn_xTi_{0.5}Fe_{23}O_{41}$ ($0.0 \le x \le 1.2$): *1* – region of EMC existence, *2* – region of EMP existence, *3* – region of EMA existence, *4* – paramagnetic state.

The value of anisotropy field H_Θ at room temperature decreases with the increase in x. According to [2], anisotropy field H_Θ changes the sign near the concentration of Zn^{2+} ions $x = 1.5$. The value of saturation magnetization increases with the increase in x [2 , 21].

CONCLUSIONS

Therefore, the present research paper suggests a technique for estimation of magnetocrystalline anisotropy field values and magnetomechanical ratios from research on ferromagnetic resonance in hexaferrites with anisotropy of easy magnetization plane type.

It is shown that the substitution of the $Co^{2+}Ti^{4+}$ complex for three-valent iron ions in hexaferrite $Ba_3Co_{1.5}Fe_{24.5}O_{41}$ leads to the widening of the temperature region of EMP existence with high magnetic permeability. Anisotropy field in relation to the base plane (H_Θ) increases in this case.

Substitution of non-magnetic Zn^{2+} ions for Co^{2+} ions in hexaferrite $Ba_3Co_{2.5}Ti_{0.5}Fe_{23}O_{41}$ reduces the value of anisotropy field H_Θ. The value of saturation magnetization increases, which ought to lead to the increase in magnetic permeability [22].

This research was supported by the Tomsk State University Competitiveness Improvement Program.

REFERENCES

1. R. C. Pullar, Prog. Mat. Sci., 57, Issue 7, 1191–1334 (2012).
2. J. Smit and H. P. J. Wijn, Ferrites, Philips Technical Library, Eindhoven (1959).
3. A. A. Oshlakov, V. A. Zhuravlev, Russ. Phys. J., **43**, No. 9, 804–807 (2000).
4. V. A. Zhuravlev, E. P. Naiden, A. A. Oshlakov, Russ. Phys. J., **44**, No. 8, 806–808 (2001).
5. R. Grossinger, JMMM, **28**, 137–142 (1982).
6. G. Asti and S. Rinaldi, J. Appl. Phys., **45**, 3601–3610 (1974).
7. R. Grossinger, J. Alloys and Compounds, **369**, 5–9 (2004).
8. V. A. Zhuravlev, V. I. Itin, R. V. Minin, *et al.*, J. All. Comp., **771**, 686–698 (2019).
9. V. A. Zhuravlev and E. P. Naiden, Phys. Solid State, **51**, Iss. 2, 327–333 (2009).

10. E. Schlömann, J. Phys. Chem. Solids, **6**, 257–266 (1958).
11. E. Schlömann, J. Phys. Radium, **20**, 327 (1959).
12. E. Schlömann and R. V. Jones, J. Appl. Phys., **30**, 177 (1959).
13. V. A. Zhuravlev, J. Phys. of the Solid State, **41**, Issue 6, 956–959 (1999).
14. V. A. Zhuravlev and V. A. Meshcheryakov, Russ. Phys. J., **56**, No. 12, 1387–1397 (2014).
15. A. G. Gurevich, G. A. Melkov, Magnetization Oscillations and Waves, CRC Press (1996).
16. A. V. Zhuravlev, V. A. Zhuravlev, Software for Calculation of Magnetomechanical Ratios and Magnetic Anisotropy Fields of Polycrystalline and Powder Ferrimagnetics with Cubic, Hexagonal, Tetragonal and Trigonal Crystalline Structures from Experiments on Ferromagnetic Resonance, Right holder: National Research Tomsk State University, Registration number 2016660395, date of registration in the Computer Software Register: September 15, 2016.
17. V. A. Zhuravlev, V. A. Meshcheryakov, A. S. Shestakov, Izv. Vyssh. Uchebn. Zaved. Fiz., **55**, No. 8/2, 177–178 (2012).
18. V. Yu. Kreslin, E. P. Naiden, Instruments and Experimental Techniques, **45**, 55-60 (2002)
19. L. T. Bugaenko, S. M. Ryabykh, A. L. Bugaenko, Moscow University Chemistry Bulletin, **63**, Issue 6, 303–317 (2008).
20. D. Bonnenberg and H. P. J. Wijn, Landolt-Bornstein Numerical and Functional Relationships in Science and Technology, in: New series, Group III: Crystal and Solid State Physics, V. 4, K.-H. Hellwege and A. M. Hellwege, ed., Springer Verlag, Berlin, 593–603, Pt. B (1970).
21. X. Wang, L. Li, Z. Yue, *et al.*, JMMM, **246**, 434–439 (2002).
22. V. A. Zhuravlev and V. I. Suslyaev, Russ. Phys. J., **49**, No. 8, 840–846 (2006).